

Vol. 3 • No. 2 • February • 2019

[www.adv-biosys.com](http://www.adv-biosys.com)

# ADVANCED BIOSYSTEMS



WILEY-VCH

# Enhanced Osteogenic Differentiation of Human Mesenchymal Stem Cells Using Microbubbles and Low Intensity Pulsed Ultrasound on 3D Printed Scaffolds

Jenna Osborn, Mitra Aliabouzar, Xuan Zhou, Raj Rao, Lijie Grace Zhang, and Kausik Sarkar\*

Lipid-coated microbubbles, clinically approved as contrast enhancing agents for ultrasound imaging, are investigated for the first time for their possible applications in bone tissue engineering. Effects of microbubbles (average diameter 1.1  $\mu\text{m}$ ) coated by a mixture of lipids (1,2-dipalmitoyl-sn-glycero-3-phosphocholine, 1,2-dipalmitoyl-sn-glycero-3-phosphoethanolamine-N-[methoxy(polyethylene glycol)-2000], and 1,2-dipalmitoyl-3-trimethylammonium-propane) in the presence of low intensity pulsed ultrasound (LIPUS) on human mesenchymal stem cells seeded on 3D printed poly(lactic acid) porous scaffolds are investigated. LIPUS stimulation (30  $\text{mW cm}^{-2}$ , 1.5 MHz, 20% duty cycle) for 3 min a day with 0.5% v/v microbubbles results in a significant increase in proliferation (up to 19.3%) when compared to control after 1, 3, and 5 d. A 3-week osteogenic differentiation study shows a significant increase in total protein content (up to 27.5%), calcium deposition (up to 4.3%), and alkaline phosphatase activity (up to 43.1%) initiated by LIPUS with and without the presence of microbubbles. The microbubbles are found to remain stable during exposure, and their sustained oscillations demonstrably help focus the LIPUS energy toward enhanced cellular response. Integrating LIPUS and microbubbles promises to be a novel and effective strategy for bone tissue engineering and regeneration therapies.

## 1. Introduction

Bone lesions and defects, resulting from trauma, tumors, or infection (osteomyelitis), are worldwide health problems affecting millions of Americans.<sup>[1]</sup> These disorders are some of the main causes of pain and disabilities in the United States and account for more than 6 million hospital visits every

year.<sup>[1,2]</sup> The current treatment options for bone injuries or diseases requiring surgical interventions are autografts, allografts, and artificial implantations. All suffer from significant shortcomings, e.g., insufficient donor tissue availability for autografts, risk of potential immunological rejection for allografts, and lack of proper integration with host tissues, and therefore, multiple surgeries for artificial implantation.<sup>[2,3]</sup> With increasing incidence of these disorders, alternative strategies for bone tissue repair and regeneration are desirable.

Tissue engineering provides a promising tool for tissue repair and generation by growing tissues directly from cells in a bio-mimicking environment by providing a biocompatible scaffold with suitable growth factors and mechanical cues.<sup>[4]</sup> Human mesenchymal stem cells (hMSCs) have been widely investigated as a potential cell source for bone tissue engineering.<sup>[5]</sup> The advantage of the hMSCs lies in their ability to differentiate into a variety of cell types, such as osteoblasts, chondrocytes, or adipocytes when exposed

to proper environmental and chemical factors.<sup>[6,7]</sup> 3D printing has emerged as a novel means for constructing a proper environment and patient injury-specific scaffolds for replacements and grafts.<sup>[7,8]</sup> The scaffolds can be printed from biodegradable materials using computer-assisted design (CAD) packages using CT or MRI images of the injury site. 3D printed structures with controllable pore sizes could also be custom designed to mimic the in vivo microenvironment, where seeded stem cells would grow, proliferate, and differentiate into desired tissues. These constructs would be implanted into the injury sites and integrated with the host tissue as the scaffold material degrades.

A number of external factors such as ultrasound,<sup>[9–11]</sup> electromagnetic fields,<sup>[12]</sup> bone growth factors (bone morphogenic protein),<sup>[13]</sup> and medicines (Alendronate)<sup>[14]</sup> have been known to improve and promote bone cell growth and fracture healing. Traditionally, ultrasound has been utilized as a diagnostic modality. However, low intensity pulsed ultrasound (LIPUS)—intensities less than 100  $\text{mW cm}^{-2}$  and frequencies between 0.75 and 1.5 MHz—has been known to have therapeutic potentials<sup>[15]</sup> and has been approved for bone fracture healing in the United States by the Food and Drug Administration (FDA). It

J. Osborn, M. Aliabouzar, X. Zhou, Prof. R. Rao, Prof. L. G. Zhang, Prof. K. Sarkar  
Mechanical and Aerospace Engineering  
George Washington University  
Washington, DC 20052, USA  
E-mail: sarkar@gwu.edu

R. Rao  
Orthopaedic Surgery  
School of Medicine  
George Washington University  
Washington, DC 20052, USA

 The ORCID identification number(s) for the author(s) of this article can be found under <https://doi.org/10.1002/adbi.201800257>.

DOI: 10.1002/adbi.201800257

has been proposed that LIPUS induces micromechanical stimulations of bone cells and inducing osteogenesis, described by Wolff's law.<sup>[16]</sup>

There have been many in vitro experiments suggesting that LIPUS treatments induce multifunctional effects that are directly involved with bone formation and resorption varying excitation frequency, intensity, duty cycle, and duration.<sup>[16]</sup> Budhiraja et al.<sup>[9]</sup> found that exposing hMSCs to LIPUS with an excitation frequency of 5 MHz significantly increases cell proliferation. Yue et al.<sup>[17]</sup> showed that LIPUS stimulation also enhanced osteogenesis of mouse adipose-derived stem cells to LIPUS by measuring runt-related transcription factor 2 (Runx2), osterix, and osteopontin gene expression. Uddin and Qin<sup>[10]</sup> found that LIPUS restores normal osteogenic differentiation of hMSCs under simulated microgravity. We have previously shown that LIPUS can improve proliferation of hMSCs and their osteogenic<sup>[11]</sup> and chondrogenic<sup>[18]</sup> differentiation on 3D printed tissue constructs.

Due to their highly echogenic gas cores, microbubbles (MBs) coated by a monolayer of lipids, proteins, or other surface active molecules have become an FDA-approved agent for contrast enhanced ultrasound imaging.<sup>[19]</sup> Recently, microbubbles have been explored for a variety of novel biomedical applications such as drug delivery,<sup>[20]</sup> thrombolysis,<sup>[21]</sup> and blood brain barrier opening.<sup>[22]</sup> Our lab has been exploring the possibility of facilitating tissue engineering by harnessing the beneficial effects of LIPUS with applications of microbubbles. We have recently shown that LIPUS in the presence of microbubbles can significantly enhance chondrogenesis of hMSCs in vitro on a 3D printed poly(ethylene glycol)-diacrylate hydrogel scaffold—glycosaminoglycan production increased by 17% (5% by LIPUS alone) and type II collagen by 78% (44% by LIPUS alone).<sup>[23]</sup>

Here, for the first time, the effects of LIPUS in the presence of microbubbles on proliferation and osteogenic differentiation of hMSCs on 3D printed poly(lactic)-acid (PLA) scaffolds are evaluated. For the LIPUS parameters used within this study, the stability and acoustic behaviors of the microbubbles were evaluated. Within this investigation, 1, 3, and 5 d proliferation studies and 3 week osteogenic differentiation studies were performed for investigation.

## 2. Results

### 2.1. Characterization of Scaffolds

The average pore dimensions of the scaffolds were 700 and 1000  $\mu\text{m}$  as assessed by the scanning electron microscopy (SEM) images taken of the scaffolds (Figure 1a). The data collected during compression testing were converted into stress and strain and a linear fit was executed. The average Young's modulus of the scaffolds was found to be  $2.15 \pm 0.15$  MPa.

### 2.2. Microbubble Characterization and Stability

As noted before, the average diameter of the synthesized lipid-coated microbubbles is 1.1–1.2  $\mu\text{m}$  with a concentration of about  $10^8$ – $10^9$  particles per milliliter (Figure 1b). The stability and scattering ability of the microbubbles were explored over a time interval of 3 min, same as that of the cell exposure. The signals with and without microbubbles are plotted in Figure 2a. The enhancement of the scattered signal due to microbubbles plotted in Figure 2b shows no significant difference in the level of enhancement between the timepoints over the exposure time of 3 min (*t*-test gives  $p > 0.05$ ).

### 2.3. hMSC Proliferation

For the effects of LIPUS and LIPUS in the presence of 0.5% v/v microbubbles on hMSC proliferation, the percent reduction of Alamar Blue Assay was measured after 1, 3, and 5 d of treatment. The results can be seen in Figure 3 for all three groups, control, LIPUS, and LIPUS in the presence of microbubbles (LIPUS + MBs). After 1 d, there was 10.2% increase in percent reduction in Alamar Blue when the cells were exposed to LIPUS in the presence of microbubbles as compared to control ( $n = 19$ ,  $p = 0.0041$ ), while the corresponding increase with only LIPUS stimulation was 7.2%. After 3 d, the cells with LIPUS stimulation in the presence of microbubbles resulted in

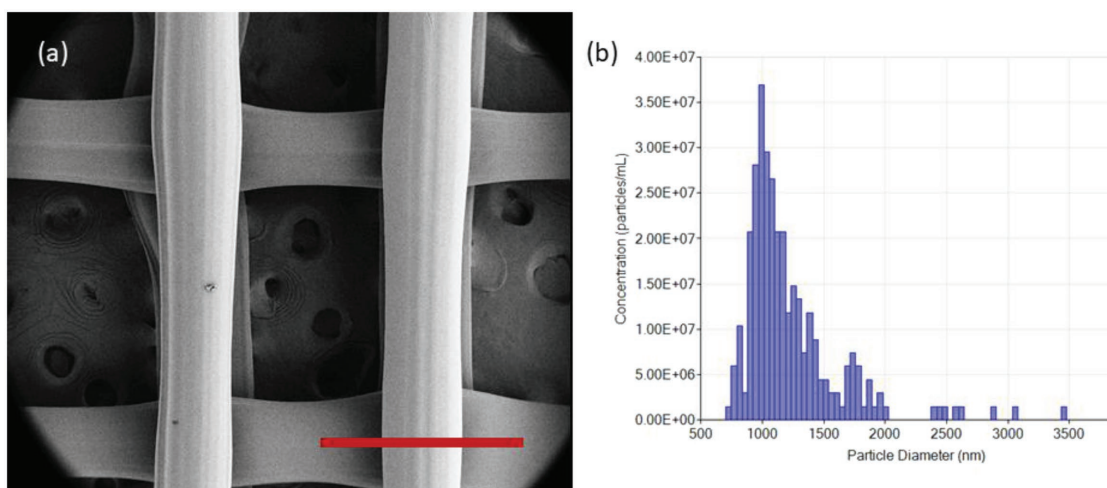


**Figure 1.** a) 3D printed PLA scaffolds visualized with SEM. The red scale bar represents 1 mm. b) Size distribution as measured by qNano of the microbubbles.

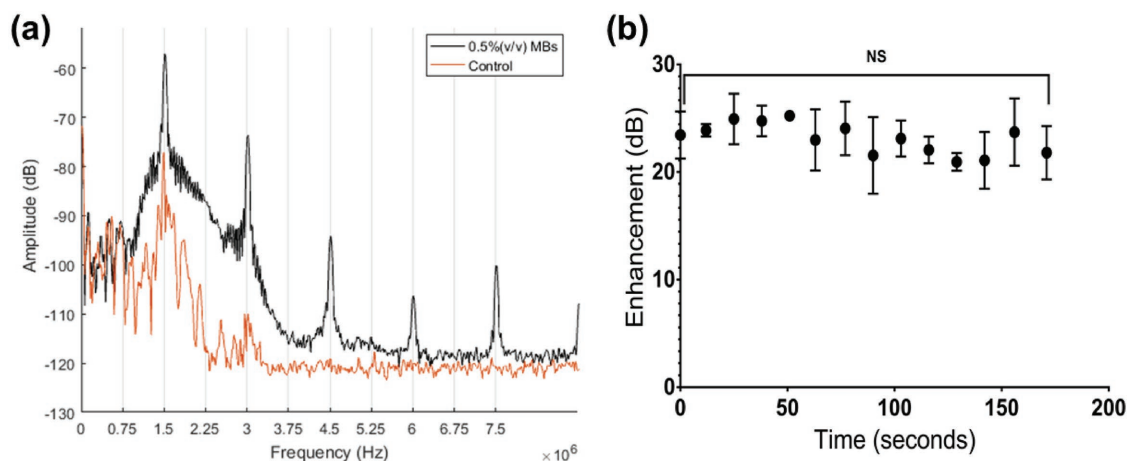


**Figure 2.** a) Frequency spectrum of the control (orange) and 0.5% v/v microbubble (MBs) solution scattered signals. b) Signal enhancement with the addition of 0.5% v/v microbubbles as compared to control at 1.5 MHz over the course of 180 s of continuous exposure ( $n = 4$ ).

a 16.3% increase in percent reduction in Alamar Blue (LIPUS alone had an 8.6% increase) compared to control ( $n = 17$ ,  $p < 0.0001$ ). After 5 d, corresponding increases are 19.3% for LIPUS in the presence of microbubbles and 4.4% with LIPUS alone ( $n = 8$ ,  $p = 0.0041$ ). The cell morphologies imaged using confocal microscopy after 3 d of exposure to LIPUS and LIPUS in the presence of microbubbles show a considerable increase in proliferation as shown in Figure 4.

#### 2.4. Osteogenic Differentiation

For osteogenic differentiation, three specific differentiation markers—total protein (Figure 5), calcium deposition (Figure 6), and alkaline phosphatase (ALP) activity (Figure 7)—were tested for 3 weeks on the same three groups—control, LIPUS, and LIPUS in the presence of microbubbles. After 3 weeks a 27.5% increase was observed for total protein content with LIPUS in the presence of MBs ( $n = 12$ ,  $p < 0.0001$ ), while with only LIPUS stimulation had a 12% increase as compared to control ( $n = 12$ ,  $p = 0.0021$ ). Extracellular calcium deposition recorded a 4.3% increase for LIPUS+MBs ( $n = 9$ ,  $p < 0.0001$ ) while with only LIPUS it was 2.2% increase ( $p = 0.0003$ ). ALP activity increases by 43.1% (25% with only LIPUS,  $p = 0.0029$ ) with LIPUS

and microbubbles after 3 weeks compared to control ( $n = 12$ ,  $p < 0.0001$ ; Figure 7).

### 3. Discussion

The scaffold developed in this study has a microenvironment and mechanical properties similar to natural cancellous bone. Bone is composed of a hard outer layer referred to as cortical bone and a spongy inner layer known as cancellous bone.<sup>[24]</sup> Cancellous bone has very high porosity ranging from 50% to 90% with voids typically of size 300  $\mu\text{m}$  to 1 mm containing bone marrow, bone cells, and fat.<sup>[24]</sup> The PLA scaffold used here has pores of comparable sizes as that of void spaces in cancellous bone. The compressive strength of the scaffold  $2.15 \pm 0.15$  MPa falls within the range 2–12 MPa of cancellous bone.<sup>[25]</sup>

For the assessment of stability and acoustic response, the microbubbles underwent 3 min of constant exposure of ultrasound under the same parameters as the cellular studies. Throughout the time exposed, the microbubbles had significantly higher scattering signals compared to control (deionized water) with enhancement as high as 25 dB. The enhancement of the scattered signal also remained relatively constant through the 3 min of exposure demonstrating that the microbubbles were stable and active under acoustic stimulation.

The proliferation of the hMSCs statistically increased over the course of 5 d of treatments when exposed to LIPUS. The addition of microbubbles further enhanced the effects of the LIPUS stimulation on proliferation. Osteogenic differentiation was also improved by the addition of LIPUS and microbubbles as visualized by three different markers, total protein content, extracellular calcium deposition, and ALP activity. A statistically significant increase in each of these differentiation markers was observed when stimulated with LIPUS in the presence of microbubbles. Total protein content, known to be related to osteogenic differentiation of hMSCs,<sup>[11]</sup> showed a 27.5% increase with LIPUS in the presence of microbubbles when compared to control after 3 weeks. With LIPUS alone, the increase was 12%. Extracellular calcium deposition is considered a late-stage

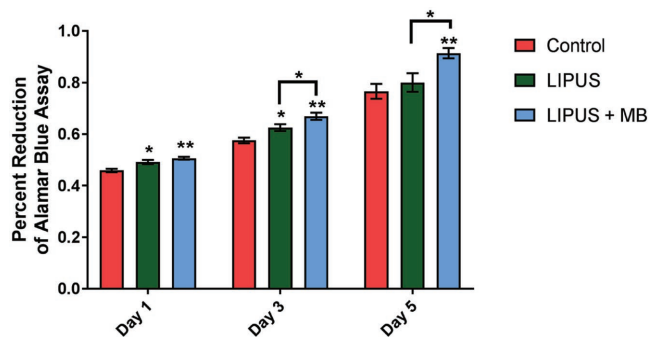


**Figure 3.** Proliferation of hMSCs on control, LIPUS, and LIPUS in the presence of microbubbles (LIPUS + MBs) groups after 1 ( $n = 19$ ), 3 ( $n = 17$ ), and 5 d ( $n = 8$ ). \* $p < 0.05$ , \*\* $p < 0.001$  compared to control group.

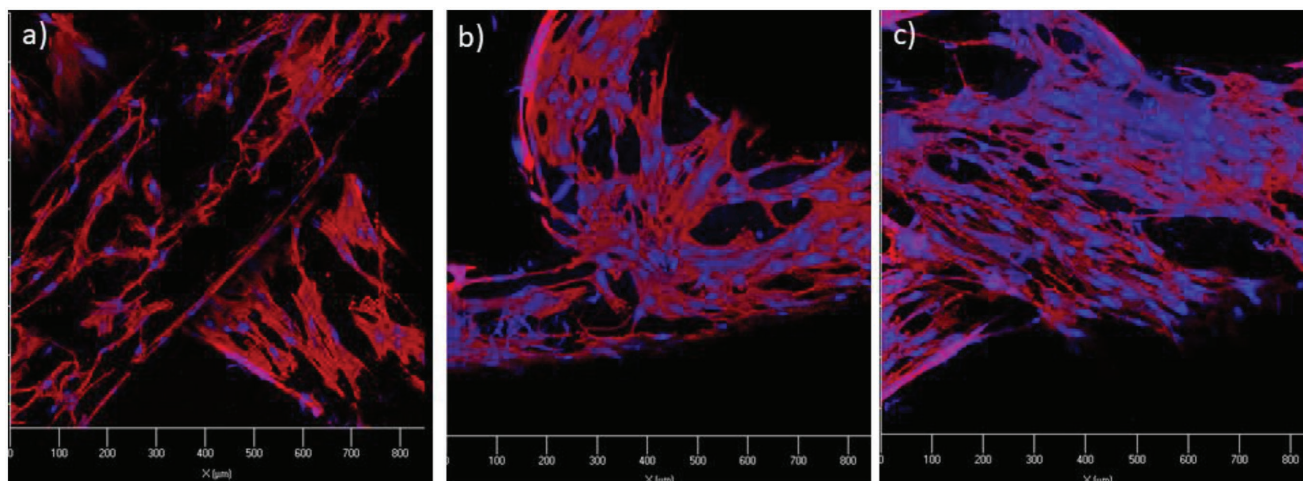


**Figure 4.** Confocal images of hMSC proliferation on 3D scaffolds with a) control, b) LIPUS, and c) LIPUS in the presence of microbubbles (LIPUS + MBs) treatment after 3 d of culture. Cytoskeleton and cell nuclei were stained by Texas Red-X phalloidin (red) and DAPI (blue), respectively.

osteogenic differentiation marker as calcium deposition has shown to be important for bone strength and stability.<sup>[26]</sup> Here, a 4.3% increase in extracellular calcium deposition was observed when exposed to LIPUS in the presence of microbubbles after 3 weeks of culture in osteogenic media. This is an improvement from the 2.2% increase when exposed to LIPUS alone. ALP is an enzyme that is critical in the formation and mineralization of the bone extracellular matrix. ALP activity is an early stage indicator of osteogenic differentiation.<sup>[11]</sup> After 3 weeks of culture, a 43.1% increase in ALP Activity was observed compared to control with LIPUS and MB, while LIPUS alone gave rise to only a 25% increase.

The mechanism behind LIPUS-stimulated cell behavior is not fully understood. The effects induced by LIPUS are believed to be nonthermal and could therefore be due to mechanical effects such as acoustic radiation forces, microstreaming, and cavitation.<sup>[27]</sup> At the low power of less than  $200 \text{ mW cm}^{-2}$  used here, one would expect negligible temperature rise.<sup>[28]</sup> Also the mechanical index ( $0.05$  at  $30 \text{ mW cm}^{-2}$  to  $0.12$  at  $200 \text{ mW cm}^{-2}$ ) is too low for strong cavitation activity<sup>[29]</sup>; thresholds for inertial cavitation in water are much higher than the acoustic parameters used here.<sup>[30]</sup> In the absence of thermal and cavitation effects at this acoustic setting, the observed bioeffects most

likely arise from the periodic normal stresses as well as shear stresses due to microstreaming.<sup>[31]</sup> LIPUS can be a source of micromechanical stress that might be responsible for bone fracture healing.<sup>[32]</sup> The micromechanical stresses have been shown to activate receptors on bone cell membranes, including integrins, mechanosensitive-calcium channels, G-proteins, IGF, TGF- $\beta$ /BMP, and gap junctions causing the induction of osteogenesis.<sup>[10]</sup> However, there is still a debate within the field as to which mechanisms are directly involved with bone formation within hMSCs. The mechanical stresses induced by LIPUS have been shown to be an effective regulator of proliferation and differentiation within hMSCs.<sup>[11,33]</sup> Budhiraja et al.<sup>[9]</sup> hypothesized that LIPUS enhanced proliferation can be attributed to the activation of the ERK1/2 and AKT pathway. Osteogenic differentiation has been proposed to be regulated by the downregulation of PPAR $\gamma$ 2 transcription factor and the upregulation of Runx2.<sup>[33]</sup> Kusuyama et al.<sup>[32]</sup> showed that osteogenesis is facilitated by ROCK-Cot/Tpl2-MEK-ERK signaling pathway and modulation of the PPAR $\gamma$ 2 activity within hMSCs. There are several pathways that LIPUS may also stimulate, such as RhoA-GTP, p-FAK, p-MEK1/2, p38 MAPK, p-IKK $\alpha/\beta$ , NK-kB, and others.<sup>[11,34]</sup> Despite the debate in the field of the exact mechanism, it is widely accepted that the addition of LIPUS

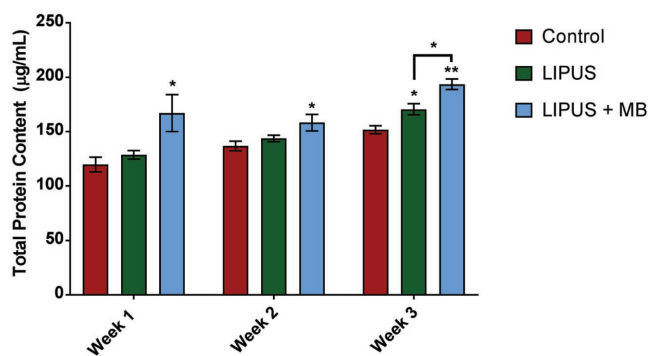


**Figure 5.** Total protein content on control, LIPUS, and LIPUS in the presence of microbubbles (LIPUS + MBs) groups after 1, 2, and 3 weeks of culture ( $n = 12$ ). \* $p < 0.05$ , \*\* $p < 0.001$  when compared to control group.

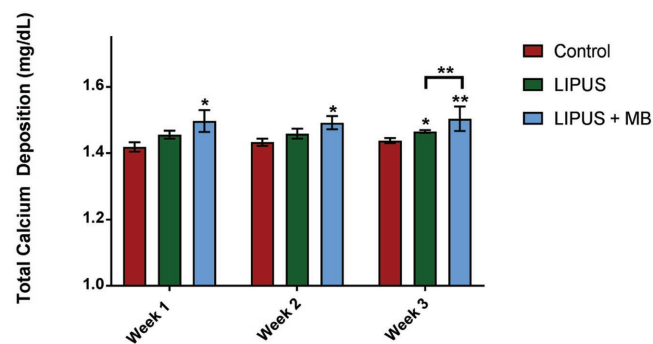


**Figure 6.** Total calcium deposition on control, LIPUS, and LIPUS in the presence of microbubbles (LIPUS + MBs) groups after 1, 3, and 5 d ( $n = 9$ ). \* $p < 0.05$ , \*\* $p < 0.001$  when compared to control group.

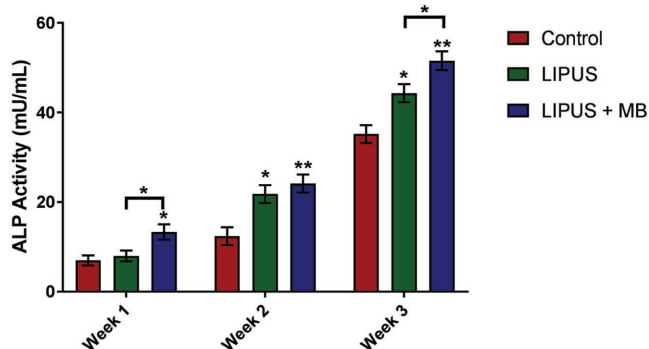


**Figure 7.** Alkaline phosphatase (ALP) activity on control, LIPUS, and LIPUS in the presence of microbubbles (LIPUS + MBs) groups after 1, 3, and 5 d ( $n = 12$ ). \* $p < 0.05$ , \*\* $p < 0.001$  when compared to control group.

has a positive impact on cell proliferation and osteogenic differentiation in hMSCs

With the addition of microbubbles to these experiments, proliferation and osteogenic differentiation markers were increased significantly suggesting that the addition can further accelerate the LIPUS effects. Due to the compressible nature of microbubbles, the gas core will expand and contract with the oscillatory pressure field of LIPUS. We showed that the microbubbles remain stable and active throughout the exposure time. The stable oscillations of the microbubbles create microstreaming—a fluid flow, around the cells creating stresses on the cell membranes of 100 Pa to 1 kPa<sup>[23]</sup>—which in turn may enhance the micromechanical stimulation on the cells caused by LIPUS. It may stimulate mechanosensitive channels or cause transient pores to develop within the cell membrane to facilitate nutrient transfer. The results support the hypothesis that the micromechanical stresses caused by microstreaming are beneficial for the enhancement of the cellular processes.

#### 4. Conclusion

Overall, LIPUS in the presence of microbubbles has shown to enhance proliferation and differentiation potential of the hMSCs as shown by total protein content, total calcium deposition, and ALP activity. After 5 d of culture, there was a 19.3% increase in percent reduction of Alamar Blue, which is proportional to cell number, as compared to control. Three osteogenic differentiation markers of the hMSCs were quantified, total protein content, extracellular calcium deposition, and ALP Activity. For the total protein content, a 27.5% increase was seen in samples treated with LIPUS in the presence of microbubbles as compared to control after 3 weeks; LIPUS stimulation alone showed a 12% increase as compared to control. For calcium deposition, there was a 4.3% increase after 3 weeks in samples exposed to LIPUS in the presence of microbubbles and a 2.2% increase in LIPUS alone. The ALP Activity increased by 43.1% after 3 weeks of culture in the samples exposed to LIPUS in the presence of microbubbles, while LIPUS increased by 25%. The addition of LIPUS in the presence of microbubbles shows to be a promising enhancement of the osteogenic differentiation

of hMSCs and could be a promising strategy for future bone tissue engineering applications.

#### 5. Experimental Section

**Production and Characterization of Scaffolds:** A fused deposition modeling (Solidoodle, NY) technique was used to 3D-print scaffolds using 1.75 mm diameter PLA filaments. First, a 3D CAD model (Rhino 6, Seattle, WA) of the shape of the scaffold was made with the appropriate dimensions (12 mm diameter disks with 1 mm thickness). Then, the infill density, scaffold pore geometry, and the speed of the printer nozzle were set using Slic3r computer numerical control conversion software. The resulting stereolithography (STL) file was exported and loaded into the Pronterface open-source software for control of the 3D printer. Rectilinear pores were chosen, which was previously shown to be optimal for hMSC growth.<sup>[18]</sup> The disk-shaped scaffolds were composed of three layers each of 0.3–0.4 mm in height and a 40% infill density. The printer nozzle was maintained at 200 °C to melt the PLA filament for printing, extruded through a 0.5 mm nozzle, and a print speed of 20 mm s<sup>-1</sup> was maintained. To assess the pore size, the scaffolds were imaged using SEM (Zeiss Nvision) as seen in Figure 1a. Compression testing was performed on the scaffolds using a mechanical testing machine (Applied Test Systems, Butler, PA). The scaffolds were compressed at a constant rate of 0.5 mm min<sup>-1</sup> while the load and head displacement were recorded through the experiment.

**Synthesis of Microbubbles:** The microbubbles used in this experiment were prepared in the lab using a lipid shell and perfluorocarbon gas. A mixture of lipids—0.75 mg mL<sup>-1</sup> of 1,2-dipalmitoyl-sn-glycero-3-phosphocholine, 1.5 mg mL<sup>-1</sup> of 1,2-dipalmitoyl-sn-glycero-3-phosphoethanolamine-*N*-[methoxy(polyethylene glycol)-2000], and 3.0 mg mL<sup>-1</sup> of 1,2-dipalmitoyl-3-trimethylammonium-propane (Avanti, AL)—was dissolved in heated (45 °C) propylene glycol for 30 min. Glycerol and phosphate buffer solution (PBS) were separately heated and then added to the lipid mixture while heated for 40 min. The solution was kept at 4 °C overnight. The following day, 1.5 mL of the lipid solution was placed in a 2 mL glass vial, crimp-closed, and the remaining headspace underwent gas exchange with perfluorobutane (Fluoromed, TX). The microbubbles were generated by mechanical agitation of the vial for 45 s using a Vial Mixer (Bristol Myers Squibb). The resulting microbubbles were highly polydisperse in size. To narrow the range of diameters, the suspension was diluted to 50 mL in PBS and centrifuged at 40 relative centrifugal force for 4 min using a bucket-rotor centrifuge. Of the 50 mL of the centrifuged solution, the first 15 mL was discarded to eliminate the larger microbubbles and the second 15 mL was used for the experiments. To determine the average diameter and concentration of the microbubbles within the isolated volume, the size distribution was measured using qNano (Izon Science, MA) with nanopore membrane NP2000 (1000–5000 nm). The average size was found to be roughly 1.1–1.2 μm with an average concentration of about 10<sup>8</sup>–10<sup>9</sup> particles per milliliter. The size distribution of the centrifuged microbubbles is plotted in Figure 1b.

**Characterization of Microbubble Stability and Acoustic Response:** The stability and acoustic response of the microbubbles were evaluated under 3 min of continuous acoustic excitation. Two perpendicularly aligned spherically focused transducers with the same specifications (diameter 12.7 mm, central frequency 2.25 MHz with -6 dB: 1.48–2.90 MHz, focal distance of 30.48 mm) (Olympus NDT, Waltham, MA) were used for the assessment of microbubble acoustic properties (Figure 8). Both transducers were calibrated using a 0.4 mm needle hydrophone (HNC400, ONDA, Sunnyvale, CA) in a water tank filled with degassed deionized water. The polycarbonate chamber (50 mm × 50 mm × 45 mm) was filled with 0.5% v/v microbubbles in deionized water. Control experiments were performed in identical setup without microbubbles. An ultrasound pulse was generated by a programmable function generator (33250A, Agilent, Palo Alto, CA, USA), which was amplified by a broadband 55 dB radio frequency (RF) power amplifier to excite the immersion transmitting transducer. The excitation parameters

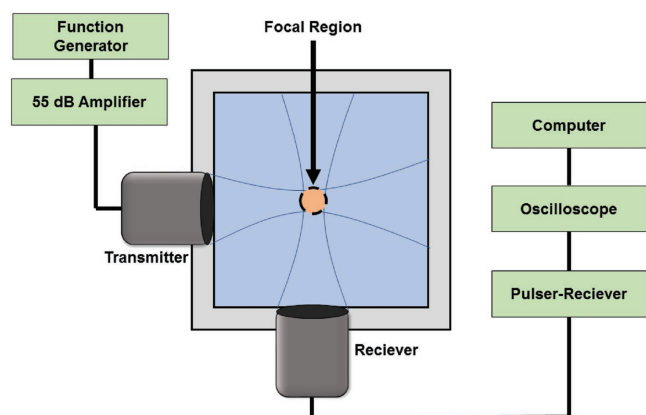


**Figure 8.** Experimental setup for the assessment of microbubble stability and acoustic response.

for the transmitting transducer were 1.5 MHz, 30 mW cm<sup>-2</sup> spatial average temporal average intensity, 32 cycles, and a pulse repetition frequency of 100 Hz. The receiving transducer was connected to a pulser-receiver (model 5800, Panametrics-NDT, Waltham, MA), which was connected to an oscilloscope. The signals were averaged over 64 signals and were taken with a custom-written MATLAB (Mathworks, Natick, MA) program for 50 replicates. A fast Fourier transform was taken of the signals. The signals were assessed over 3 min of continuous exposure to evaluate the stability of the microbubbles over the same time length of cell excitation. This was repeated four times and assessed for a statistically significant difference between the first measurement ( $t = 0$  s) and last measurement ( $t = 171$  s).

**Ultrasound Parameters:** The ultrasound parameters for hMSC parameters were optimized previously for cell proliferation by Aliabouzar et al.<sup>[23]</sup> The schematic representation of ultrasound exposure setup is presented in **Figure 9**. Briefly, the ultrasound pulse produced by a programmable function generator (33250A, Agilent, Palo Alto, CA, USA) and amplified by a broadband 55 dB laboratory RF power amplifier (model A-150, ENI, Rochester, NY, USA) was used to excite a single element unfocused immersion transducer (diameter 12.7 mm, central frequency 2.25 MHz with  $-6$  dB: 1.48–2.90 MHz) (Olympus NDT, Waltham, MA). A sterilized (with 70% ethanol and 1 h ultraviolet exposure) XYZ positioning stage (Newport Corp., CA) was used to hold the transducer vertically in the well of the cell culture plate touching the top surface of the media there. The separation of the head of 13 mm from the cells at the well bottom places the cells within the nominal near-field distance (40.3 mm at 1.5 MHz) as in previous studies.<sup>[11,23,35,36]</sup> However, it is to be noted that animal and clinical trials of therapeutic ultrasound typically involve near-field stimulation by transducers in direct contact with the skin.<sup>[37]</sup> Moreover, Li et al.<sup>[35]</sup> found the optimum intensity of ultrasound stimulation in a far-field setup (exposure distance of 240 mm) to be identical to that found in a near-field setup (5 mm) by Parvizi et al.<sup>[38]</sup> The acoustic field was recently investigated in this setup examining its axial and radial variations as well as effects due to the plastic walls of the cell culture plate.<sup>[18]</sup> The field was found to be satisfactory; there were negligible spatial variation, no reflection and minimal effects of standing waves. For experiments in the presence of microbubbles, a mixture of culture medium and 0.5% v/v microbubbles was pipetted into each well. Each well was filled up with 3 mL of media or media and microbubble mixture, taking care that no air bubble was trapped. The working wells were separated by one empty well, i.e., every other well in the 24-well plate was used to avoid cross transfer of ultrasound energy to neighboring wells. Before experimentation, cells were washed with PBS. Cells were exposed to LIPUS at a frequency of 1.5 MHz, spatial average-temporal average intensity of 30 mW cm<sup>-2</sup>, pressure amplitude of 63.41 kPa, and a duty cycle (fraction of the time within a pulse repetition period that transducer is on) of 20% for 3 min per day. Previously, an hMSC proliferation study varying bubble

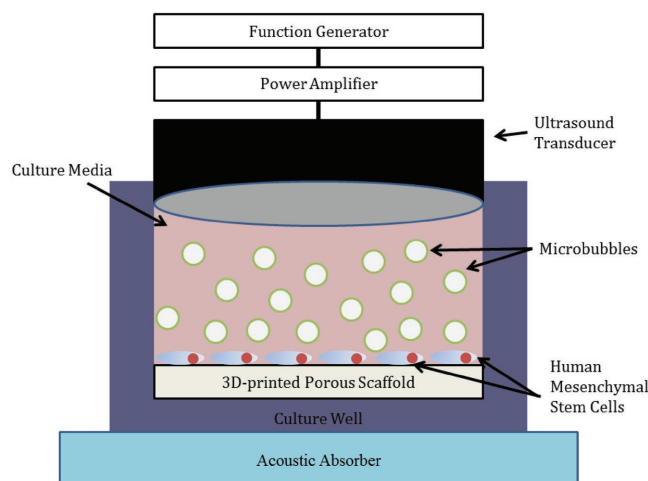


**Figure 9.** Experimental setup for ultrasound stimulation of hMSCs.

concentration and acoustic parameters (frequency, intensity, duty cycle, and duration) was performed to find the parameters used here to be roughly optimal.<sup>[18,23]</sup> Control groups underwent the same submersion and withdrawal of transducers with ultrasound power turned off.

**Cell Culture:** Under an IRB-approved protocol with written, informed consent, human bone marrow mesenchymal stem cells (hMSCs) were obtained from healthy individuals at Tulane University. The cells were characterized at the Institute for Regenerative Medicine at Texas A&M Health Science Center with a fully executed Material Transfer Agreement. Passages 3–6 were used for all experiments. The cells were cultured in  $\alpha$ -Minimum Essential Medium Eagle supplemented with 16.5% v/v fetal bovine serum (FBS), 1% v/v L-glutamine, and 1% v/v penicillin and streptomycin. The hMSCs were incubated in a 37 °C, 5% CO<sub>2</sub>, and 95% relative humidity environment. For the studies performing osteogenic differentiation of the hMSCs, the cells were cultured in Dulbecco's Modified Eagle Medium supplemented with 10% v/v FBS, 50  $\mu$ g mL<sup>-1</sup> of L-ascorbate acid, 10 mmol L<sup>-1</sup> of  $\beta$ -glycerophosphate, 10 nmol L<sup>-1</sup> of dexamethasone, and 1% v/v penicillin and streptomycin.

**Proliferation of hMSCs:** The effects of LIPUS with and without the presence of microbubbles on proliferation were evaluated. The hMSCs were cultured in 24-well plates with  $2.5 \times 10^4$  cells per well overnight. The samples were divided into three different groups, control (no LIPUS or microbubbles), LIPUS (no microbubbles), and LIPUS in the presence of microbubbles (LIPUS + MBs on figures). The cells were tested after 1, 3, and 5 d of exposure using Alamar Blue Assay. The cells were incubated for 2 h at 37 °C and then tested by spectrophotometer for absorbance at 570 and 600 nm. The absorbance measurements were converted to percent reduction of the assay using the manufacturer's instructions. To account for any effects the scaffold may have on the assay, the negative control experiments were performed with the test samples in the scaffold. The percent reduction of the assay is proportional to cell number. The cells were rinsed with PBS three times and replenished with fresh medium.

After 3 d of treatment, cell morphology of each group was imaged by confocal microscopy (Carl Zeiss LSM 710). The samples were washed with PBS twice and fixed with 10% formalin for 10 min. The samples were washed and then underwent permeabilization via 0.1% Triton-100 for 10 min. The samples were stained with Texas Red for 1 h and 4',6-diamidino-2-phenylindole (DAPI) for 5 min.

**Osteogenic Differentiation of hMSCs:** For osteogenic differentiation studies, the hMSCs were cultured in 24-well plates with roughly  $1 \times 10^5$  cells per well overnight. The cells were divided into the same three groups and were then immersed in osteogenic media and exposed to ultrasound with the parameters mentioned above for 3 d. After that, the cells were incubated in osteogenic media for 1, 2, or 3 weeks. The samples were lysed using a freeze-thaw cycling method three times and

then were evaluated for total protein content, calcium deposition, and ALP. Total protein content was tested using a commercial BCA Protein Assay Reagent Kit (Pierce Biotechnology) and the concentrations of the samples were compared to a standard curve of bovine serum albumin of varying concentration. Calcium deposition was tested using a standard assay kit (Pointe Scientific, Canton, MI) according to the manufacturer instructions and compared to a calcium standard with a known concentration. ALP activity was tested using a standard assay kit (Bioquest, Sunnydale, CA) according to the manufacturer instructions, comparing the results to a standard curve to determine the concentration.

**Statistical Analysis:** For the statistical evaluation of all studies, a one-way analysis of variance was used to determine statistical significance. A *p*-value of less than 0.05 was taken to be significant. A Tukey's range test was performed to determine significance between individual groups, and *p* < 0.05 was taken to be significant. All data are presented as mean ± standard error of the mean. A D'Agostino and Pearson test was performed on the data to ensure a normal distribution. To ensure equal variances between groups, a Brown–Forsythe test was performed. Data processing was performed using GraphPad Prism 7 (GraphPad Software, La Jolla, CA).

## Acknowledgements

The authors would like to thank GW Nanofabrication and Imaging Facility for their help in this study. This work was supported by the George Washington University CDRF.

## Conflict of Interest

The authors declare no conflict of interest.

## Keywords

microbubbles, osteogenesis, stem cells, tissue engineering, ultrasound

Received: August 27, 2018

Revised: October 8, 2018

Published online:

- [1] A. Piroso, R. Gottardi, P. G. Alexander, R. S. Tuan, *Stem Cell Res. Ther.* **2018**, *9*, 112.
- [2] R. Agarwal, A. J. García, *Adv. Drug Delivery Rev.* **2015**, *94*, 53.
- [3] F. Loi, L. A. Córdova, J. Pajarinen, T.-H. Lin, Z. Yao, S. B. Goodman, *Bone* **2016**, *86*, 119.
- [4] S. Bose, S. Vahabzadeh, A. Bandyopadhyay, *Mater. Today* **2013**, *16*, 496.
- [5] H. Petite, V. Viateau, W. Bensaïd, A. Meunier, C. de Pollak, M. Bourguignon, K. Oudina, L. Sedel, G. Guillemin, *Nat. Biotechnol.* **2000**, *18*, 959.
- [6] M. F. Pittenger, A. M. Mackay, S. C. Beck, R. K. Jaiswal, R. Douglas, J. D. Mosca, M. A. Moorman, D. W. Simonetti, S. Craig, D. R. Marshak, *Science* **1999**, *284*, 143.
- [7] X. Zhou, M. Nowicki, H. Cui, W. Zhu, X. Fang, S. Miao, S.-J. Lee, M. Keidar, L. G. Zhang, *Carbon* **2017**, *116*, 615.
- [8] a) X. Zhou, W. Zhu, M. Nowicki, S. Miao, H. Cui, B. Holmes, R. I. Glazer, L. G. Zhang, *ACS Appl. Mater. Interfaces* **2016**, *8*, 30017; b) X. Zhou, H. Cui, M. Nowicki, S. Miao, S.-J. Lee, F. Masood, B. T. Harris, L. G. Zhang, *ACS Appl. Mater. Interfaces* **2018**, *10*, 8993.
- [9] G. Budhiraja, N. Sahu, A. Subramanian, *Biotechnol. J.* **2018**, *13*, 1700382.
- [10] S. M. Z. Uddin, Y.-X. Qin, *PLoS One* **2013**, *8*, e73914.
- [11] X. Zhou, N. J. Castro, W. Zhu, H. Cui, M. Aliabouzar, K. Sarkar, L. G. Zhang, *Sci. Rep.* **2016**, *6*, 32876.
- [12] J. Ryaby, *Clin. Orthop. Relat. Res.* **1998**, *355*, S205.
- [13] V. Rahman Cheryl, D. Ben-David, A. Dhillon, G. Kuhn, W. A. Gould Toby, R. Müller, R. A. J. Rose Felicity, M. Shakesheff Kevin, E. Livne, *J. Tissue Eng. Regen. Med.* **2014**, *8*, 59.
- [14] U. A. Liberman, S. R. Weiss, J. Bröll, H. W. Minne, H. Quan, N. H. Bell, J. Rodriguez-Portales, R. W. Downs, J. Dequeker, M. Favus, E. Seeman, R. R. Recker, T. Capizzi, A. C. Santora, A. Lombardi, R. V. Shah, L. J. Hirsch, D. B. Karpf, *N. Engl. J. Med.* **1995**, *333*, 1437.
- [15] K. Sena, S. R. Angle, A. Kanaji, C. Aher, D. G. Karwo, D. R. Sumner, A. S. Virdi, *Ultrasonics* **2011**, *51*, 639.
- [16] K. Lim, J. Kim, H. Seonwoo, S. H. Park, P.-H. Choung, J. H. Chung, *BioMed Res. Int.* **2013**, *2013*, 15.
- [17] Y. Yue, X. Yang, X. Wei, J. Chen, N. Fu, Y. Fu, K. Ba, G. Li, Y. Yao, C. Liang, J. Zhang, X. Cai, M. Wang, *Cell Proliferation* **2013**, *46*, 320.
- [18] M. Aliabouzar, S. J. Lee, X. Zhou, G. L. J. Zhang, K. Sarkar, *Bio-technol. Bioeng.* **2018**, *115*, 495.
- [19] F. Fuechsel, D. Cosgrove, in *Ultrasound Contrast Agents: Basic Principles and Clinical Applications* (Eds: B. B. Goldberg, J. S. Raichlen, F. Forsberg), Martin Dunitz, London **2001**, pp. 327–334.
- [20] a) E. C. Unger, T. Porter, W. Culp, R. Labell, T. Matsunaga, R. Zutshi, *Adv. Drug Delivery Rev.* **2004**, *56*, 1291; b) S. Paul, R. Nahire, S. Mallik, K. Sarkar, *Comput. Mech.* **2014**, *53*, 413.
- [21] S. D. Tiukinhoy-Laing, S. L. Huang, M. Klegerman, C. K. Holland, D. D. McPherson, *Thromb. Res.* **2007**, *119*, 777.
- [22] Y. Z. Zhao, C. T. Lu, X. K. Li, J. Cai, *Expert Opin. Drug Delivery* **2013**, *10*, 987.
- [23] M. Aliabouzar, L. G. Zhang, K. Sarkar, *Sci. Rep.* **2016**, *6*, 37728.
- [24] E. Hamed, I. Jasiuk, A. Yoo, Y. Lee, T. Liszka, *J. R. Soc., Interface* **2012**, *9*, 1654.
- [25] J. Henkel, M. A. Woodruff, D. R. Epari, R. Steck, V. Glatt, I. C. Dickinson, P. F. M. Choong, M. A. Schuetz, D. W. Hutmacher, *Bone Res.* **2013**, *1*, 216.
- [26] R. Mundi, S. Petis, R. Kaloty, V. Shetty, M. Bhandari, *Indian J. Orthop.* **2009**, *43*, 132.
- [27] M. Dyson, *Br. J. Cancer Suppl.* **1982**, *5*, 165.
- [28] a) L. Claes, B. Willie, *Prog. Biophys. Mol. Biol.* **2007**, *93*, 384; b) L. Duarte, *Arch. Orthop. Trauma. Surg.* **1983**, *101*, 153.
- [29] A. Katiyar, R. L. Duncan, K. Sarkar, *J. Ther. Ultrasound* **2014**, *2*, 1.
- [30] a) C. Hill, *J. Acoust. Soc. Am.* **1972**, *52*, 667; b) E. Neppiras, *Ultrasonics* **1965**, *3*, 9; c) R. E. Apfel, *J. Acoust. Soc. Am.* **1970**, *48*, 1179.
- [31] a) H. Starritt, F. Duck, V. Humphrey, *Ultrasound Med. Biol.* **1989**, *15*, 363; b) F. Dunn, *Radiat. Environ. Biophys.* **1985**, *24*, 131; c) G. ter Haar, in *Ultrasound: Medical Applications, Biological Effects, and Hazard Potential*, (Eds: M. H. Repacholi, M. Grandolfo, A. Alessandro) Springer, Boston **1987**, p. 105.
- [32] J. Kusuyama, K. Bandow, M. Shamoto, K. Kakimoto, T. Ohnishi, T. Matsuguchi, *J. Biol. Chem.* **2014**, *289*, 10330.
- [33] R. Marom, I. Shur, R. Solomon, D. Benayahu, *J. Cell. Physiol.* **2005**, *202*, 41.
- [34] K. Ikeda, T. Takayama, N. Suzuki, K. Shimada, K. Otsuka, K. Ito, *Life Sci.* **2006**, *79*, 1936.
- [35] J. G.-R. Li, W. H.-S. Chang, J. C.-A. Lin, J.-S. Sun, *Ultrasound Med. Biol.* **2002**, *28*, 683.
- [36] a) N. Doan, P. Reher, S. Meghji, M. Harris, *J. Oral Maxillofac. Surg.* **1999**, *57*, 409; b) A. Suzuki, T. Takayama, N. Suzuki, M. Sato, T. Fukuda, K. Ito, *Acta Biochim. Biophys. Sin.* **2009**, *41*, 108.
- [37] a) J. D. Heckman, J. P. Ryaby, J. McCabe, J. J. Frey, R. F. Kilcoyne, *J. Bone Joint Surg.* **1994**, *76*, 26; b) E. Mayr, V. Frankel, A. Rüter, *Arch. Orthop. Trauma. Surg.* **2000**, *120*, 1.
- [38] J. Parvizi, C.-C. Wu, D. G. Lewallen, J. F. Greenleaf, M. E. Bolander, *J. Orthop. Res.* **1999**, *17*, 488.